PARTITIONING OF U, Zr AND FP BETWEEN MOLTEN OXIDIC AND METALLIC CORIUM

Asmolov V.G.[1], Bechta S.V.[2], Khabensky V.B.[2], Gusarov V.V.[3], Vishnevsky V.Yu.[4], Degaltsev Yu.A.[1], Abalin S.S.[1], Krushinov E.V.[2], Vitol S.A.[2], Almjashev V.I.[3], Kotova S. Yu.[2], Zagryazkin V.N.[1], Dyakov E.K.[4], Strizhov V.F.[5] and Kiselev N.P.[1]

[1] Russian Research Centre "Kourchatov Institute" (RRC KI), Moscow
[2] A.P. Alexandrov Research Institute of Technology (NITI), Sosnovy Bor
[3] Institute of Silicate Chemistry of Russian Academy of Science (ISC of RAS), St. Petersburg
[4] Luch Scientific Production Association, Podolsk, Russia
[5] Nuclear Safety Institute (IBRAE) Russian Academy of Sciences, Moscow

Abstract

Interaction of molten corium and liquid iron/stainless steel has been studied in different tests of the MASCA-1 program. These tests utilized the technology of induction melting in a cold crucible. The masses of tested corium were approximately 0.5, 2 and 100 kg. Representative quantities of Mo, Ru, SrO, BaO, CeO_2 and La_2O_3 served as fission product simulants.
After the suboxidized melt - steel interaction U and Zr have been found in the metallic phase.
To quantify the partitioning of Zr, U and fission products an extensive experimental program has been performed. The following key parameters have been identified: oxygen potential in the melt (degree of Zr-oxidation), the corium/steel mass ratio and U/Zr ratio. The paper discusses the influence of these parameters on the partitioning of the main species.

Introduction

In the progression of a light water reactor severe accident, which is accompanied by a long-term drying of the core, a molten pool is formed on the bottom of reactor vessel. All available studies of the in-vessel melt retention consider the two-layer pool as the final melt structure; it has an oxidic melt of U and Zr in the bottom part and molten steel as the surface layer. As an example we can mention studies carried out for NPP Loviisa with VVER-440 [1], AP-600 [2], and VVER-640 [3]. The molten pool thermohydraulics, which is responsible for the distribution of thermal load across the vessel, has been studied both experimentally, e.g. [4-6] and by numeric modeling of the mentioned molten pool structure. Same molten pool structure was assumed even for the studies of DNB on the external surface of the bottom, which was inferred from the distribution of heat fluxes, [7].

The surface position of the molten steel layer follows from comparison of its density, which does not exceed 7.0 g/cm^3, and oxidic U-Zr melt density, which in accordance with experimental data [8], if the U-Zr ratio is 1.2 and temperature - 2450...2700°C, amounts to ≥ 7.4 g/cm^3. It is clear that this reasoning applies only if the mentioned melts form the system with a limited reciprocal solubility. But as early as in the experiments conducted by P. Hofmann [9] it was found that large quantities U and Zr were present in the metallic part of the ingot, which had been produced by the crystallization of molten uranium dioxide, Zircaloy and steel. Even for a more simple system, U-Zr-O, under certain conditions

the melt stratification was observed, at which two liquids having different U and Zr concentrations and different densities were formed [10].

These examples testify physico-chemical processes, which take place in high-temperature melts containing $(U,Zr)O_{2-x}$ and steel (Fe). These phenomena should be taken into account in the in-vessel retention analysis, because they are likely to influence the composition, properties and mass ratio of metallic and oxidic liquids and, eventually, the retained molten pool structure. Therefore the existing forecasts of heat load distribution along the vessel bottom can be modified. The molten pool characteristics are important not only for the analysis of in-vessel corium retention, but also for its ex-vessel localization, because, along with other factors, they enable to identify the melt release scenario.

The current experimental study of corium melt–steel interaction was aimed at the determination of qualitative and quantitative characteristics of main species and FP partitioning between oxidic and metallic phases. The tests were carried out in the framework of MASCA-1 program with different corium oxidation degree, U-Zr ratio and mass fraction of iron (steel). FP partitioning have an influence on decay heat distribution in the molten pool and FP release.

1. Experimental Procedure

The method of induction melting in the cold crucible (IMCC) was used in all the experiments on the oxidic melt-iron (steel) interaction, including tests with FP simulants addition. The tests were conducted in high purity argon on the following experimental facilities:

- Small-scale facility STFM of NPO "Luch"; the melt mass ~ 0,5 kg (STFM-Fe and STFM-FP series).
- Medium-scale facility Rasplav-3 of NITI; the melt mass ~ 2 kg (MA series).
- Large-scale facility RCW in the Kurchatov Institute; the melt mass ~ 100 kg.

In accordance with the experimental procedure of STFM-Fe and STFM-FP series the sintered corium briquettes of a specified composition were slowly heated (20...25 min.) up to the required temperature, 2500...2600°C, at which they were exposed during ~ 10 min. After this iron (in some tests - stainless steel) was added, the resulting oxidic-metallic melt was exposed during 10...60 min, after that the temperature was slowly reduced to ~ 1800°C and heating was disconnected. STFM-FP tests were different from STFM-Fe by the initial charge composition, which had simulants of low-volatile FP (Mo, Ru, Sr, Ba, La, Ce) in the form of Mo, Ru, $SrCO_3$, BaO_2, La_2O_3 and CeO_2 with the concentration of 0.4 w % from the total mass of the charge. The following parameters were varied in these tests (Table 1): temperature, interaction period, metal (iron or stainless steel), U/Zr ratio, initial degree of Zr (Cn) oxidation, relative initial mass of steel (M_{st}^0 / M_Σ).

In accordance with the experimental procedure of the MA series the charge consisting of oxidic powder and metallic Zr rods was molten and superheated up to 2400...2500°C, stainless steel was introduced into the melt stepwise, the melt was exposed during 30 min., after which the generator was disconnected. In MA-3, MA-4 the charge included FP simulants: Mo, Ru, La_2O_3, CeO_2 and Ba, Sr 'metazirconates' prepared from BaO and $Sr(OH)_2 \cdot 8H_2O$ by their sintering with ZrO_2. The content of each FP stimulant was ~ 0.5 w% from the total mass of the charge. The experimental matrix of MA series is presented in Table 2.

Table 1. STFM-Fe and STFM-FP experimental matrix

Test	T, °C	Exposition time, min	Metal	U/Zr, at	Cn	M_{st}^0/M_Σ, %
STFM-Fe2	2500	10	Iron	1.15	32.6	1.84
STFM-Fe3	2500	30	Iron	1.15	32.6	1.59
STFM-Fe4	2500	30	Iron	1.16	33.4	4.36
STFM-Fe5	2500	60	Iron	1.15	32.6	1.29
STFM-Fe6	2550	10	Iron	1.20	54.6	1.57
STFM-Fe7	2600	10	Iron	1.19	69.2	1.52
STFM-Fe9	2500	30	Iron	1.14	35.6	9.52
STFM-Fe10	2600	30	Iron	1.19	69.2	4.30
STFM-Fe14	2500	30	Iron	1.14	35.6	15.22
STFM-Fe15	2500	30	SS	1.14	35.6	11.26
STFM-FP1	2600	15	Iron	1.17	44.6	3.86
STFM- FP2	2600	15	Iron	1.17	44.6	3.32
STFM- FP3	2700	15	Iron	1.17	44.6	3.71
STFM- FP6	2600	15	SS	1.17	45.5	3.82
STFM- FP7	2600	15	Iron	1.19	59.5	2.84
STFM- FP8	2600	15	Iron	1.18	62.4	2.79

Table 2. MA experimental matrix

Test	T, °C	Exposition time, min	Metal	U/Zr, at	Cn	M_{st}^0/M_Σ, %
MA-1	2500	30	SS	1.45	33.1	11.42
MA-2	2500	30	SS	1.28	74.5	10.80
MA-3	2500	30	SS	1.14	36.5	10.78
MA-4	2500	30	SS	1.17	39.7	19.09

In the large-scale test RCW a special methodology was used. Its results will be presented separately; the current paper does not give their overview.

2. Identification of Critical Parameters

In order to fulfill the experimental tasks and determine quantitative characteristics of species partitioning between oxidic and metallic phases the identification of the directly interacting molten part of the charge was of primary importance.

In the STFM tests the ingot and crusts were weighed. The charge mass, which had not participated in the interaction, was determined with adequate accuracy, After that the ingot was split and its metallic part was extracted, separated from the corium shell and weighed. In this way the total mass of interacted melt and, separately, masses of oxidic and metallic parts, which had been formed in the process of interaction, were determined.

In the MA tests the total mass of interacting melt was determined as the difference between the mass of initial charge and collected and weighed products, which had not taken part in the interaction, i.e. unmolten charge and crusts. The separate masses of metallic and oxidic parts of the ingot were determined in a way similar to the STFM tests. In all the tests the mass imbalance between the charge and the molten products collected after the test did not exceed 1.5%.

The initial composition of corium melt was calculated from the concentration of components in the oxidic and metallic ingot parts determined from the analyses, they were recalculated for their masses minus the mass of steel species present in the compositions of both parts.

In the STFM tests the content of main species was determined using standard chemical methods, and oxygen content – from the residue. In some tests Zr oxidation degree in the oxidic part was determined by direct measurements of free Zr. In the STFM-FP tests the content of FP simulants was determined by the plasma emission spectral method.

In the MA tests the composition of main species was determined by the XRF (for the oxidic part – from the average sample), oxygen in the oxidic part of the ingot – from the residue, and in the metallic part of the ingot – by the spark source mass spectrometry (SS MS). In the MA-3, MA-4 tests the content of FP simulants was determined by the mass spectrometry with inductively coupled plasma (ICP MC).

The errors of experimental data are connected with the errors of direct measurements, of the interacting corium and steel mass identification, of the evaluation of species partitioning between oxidic and metallic phases and in averaging.

The relative error of the main species content does not exceed 5% (oxygen in the metallic phase – 10%). Error of the Zr final oxidation degree does not exceed 10%. Error of the FP partitioning coefficient between oxidic and metallic phases for Mo and Ru is below 40%, and for Sr, Ba, Ce, La – below 60%.

Methodological errors caused by the species partitioning between the oxidic and metallic corium in the course of ingot crystallization should be mentioned separately. The thermodynamic evaluation of oxygen content in the conditions of equilibrium between phases at 2600°C gives higher values of oxygen concentration in the metallic phase [11] as compared to the post-test analysis data. This can be explained by the decreased oxygen solubility, when the melt temperature is reduced, and, especially, during the metallic melt crystallizationa [12]. During this oxygen can release from the metallic melt both to gas and oxidic phases, were it oxidizes such active reducers as U and Zr.

The density of separate ingot parts was measured by the bottle method, its relative error was 2%.

3. Experimental Results

3.1 U and Zr partitioning at the oxidic and metallic melt interaction

All post-test ingots consisted of oxidic and metallic parts. As a rule, the latter had magnetic properties. For all tests of STFM and MA series except for MA-2 the metallic part was located in the bottom part of the pool. It was most distinct in the MA series. Fig. 1 shows the ingot picture of a MA-3 test, after its extraction from the crucible, Fig. 2 – its reconstruction after the splitting.

Figure 1. MA-3 ingot

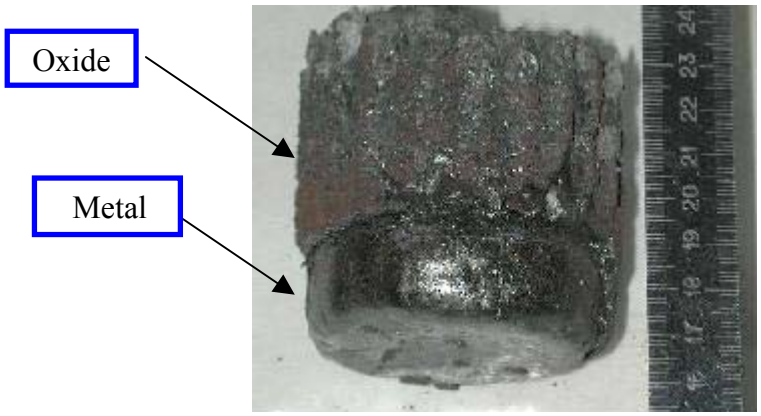

Figure 2. Reconstruction of MA-3 ingot section

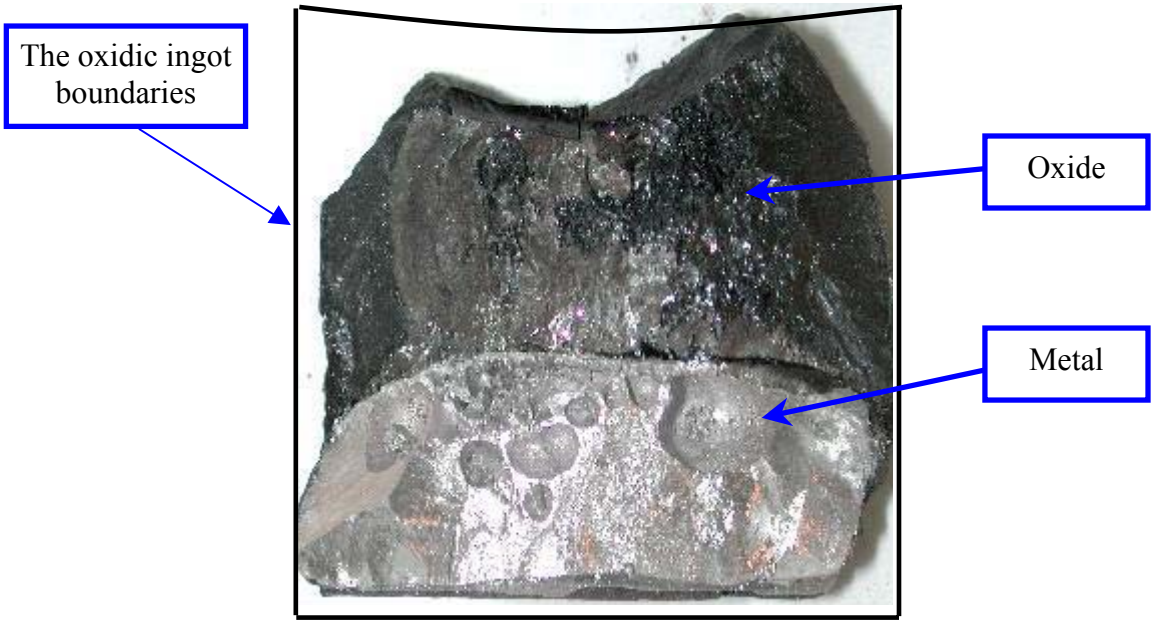

In MA-2 the metallic phase was found inside the oxidic part; it had a complex shape (Fig. 3). The top of the metallic ingot was shaped as a flattened ellipsoid, a curved “leg” was protruding from it as far as the bottom.

Figure 3. MA-2 ingot

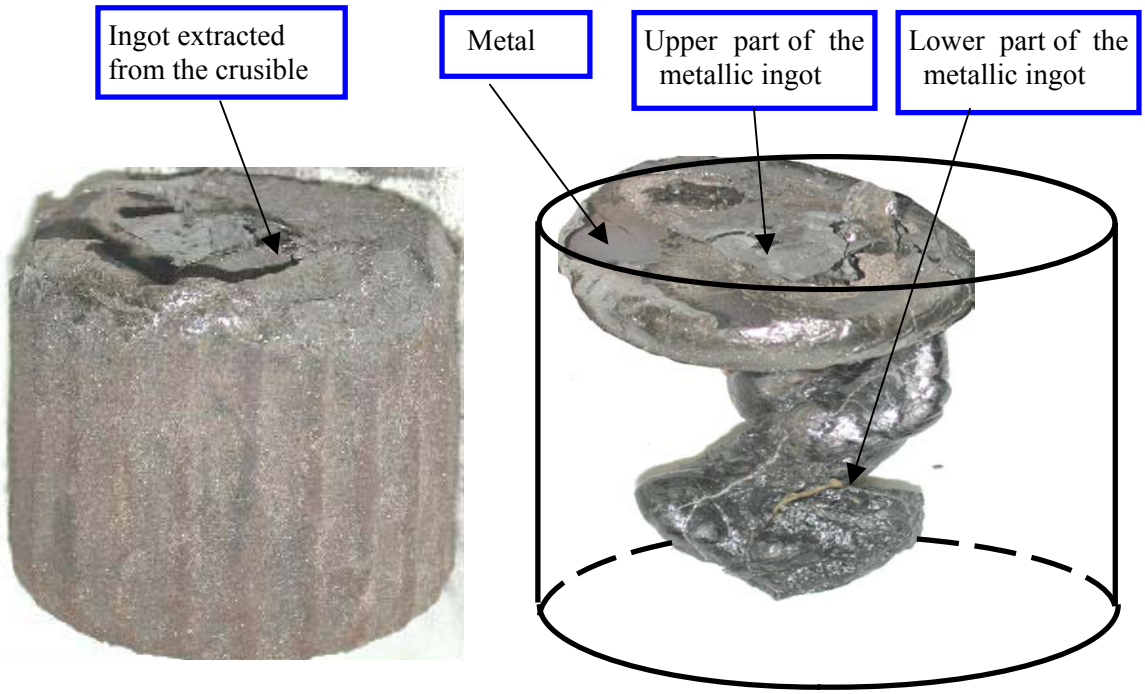

First quantitative result to be mentioned is the larger mass of formed metallic ingot than the initial mass of interacting steel and the corresponding mass decrease of the oxidic part. In order to quantify this and other phenomena we will use the following indicative parameters: the relative initial mass of steel M_{st}^0 / M_Σ and initial Zr oxidation degree as the oxidability index Cn [8]: $Cn = \frac{Zr_\Sigma - Zr_{free}}{Zr_\Sigma} \cdot 100$.

Fig. 4 shows the influence of M_{st}^0 / M_Σ on the relative mass of resulting metallic ingot M_{met}^f / M_Σ. It is evident that the transport of U and Zr from the oxidic into metallic part intensifies as the mass of steel introduced into the melt increases. The lower initial oxidation degree of Zr is, the more pronounced is this effect. The immediate influence of this factor is demonstrated in Fig. 5 for a limited range of M_{st}^0 / M_Σ. As the initial Zr oxidation degree increases, M_{met}^f / M_{st}^0 decreases.

U and Zr partitioning results in the increase of Cn in the oxidic part of the melt. As it is demonstrated in Fig. 6, the tendency of oxidic composition getting closer to C100, as long as the relative mass of introduced steel grows, is distinct for the cases with a relatively low initial oxidation degree, C30...C45. Other conditions being equal, when the initial Cn is higher, the final Cn in oxides grows too, but the insufficiency and considerable scattering of experimental data exclude their correct approximation.

Analyses of ingot compositions determined the following. Main species migrating from the suboxidized oxidic melt into the steel melt are U, Zr and O. Small amount of steel components enters the oxidic melt. Figs. 7, 8 show that U and Zr concentration in the metallic ingot decreases with the growth of initial mass fraction of steel and initial Zr oxidation degree, which is an evident manifestation of the dissolution effect.

Figure 4. Metallic fraction in the ingot as a function of the amount of introduced steel

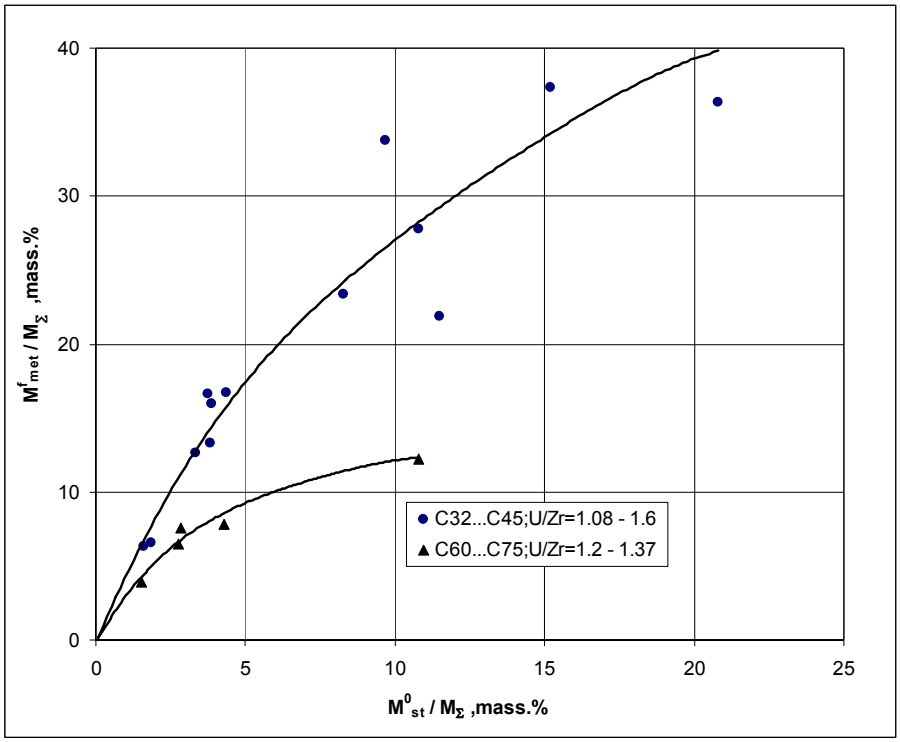

Figure 5. Relative mass of the metallic ingot as a function of initial Cn

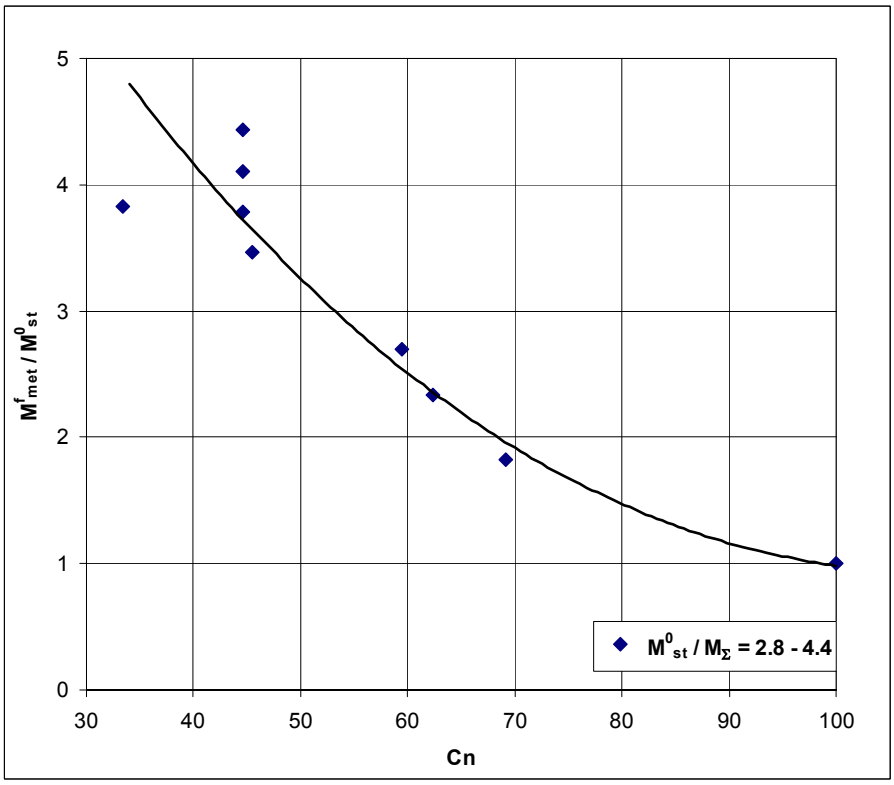

Figure 6. Final Cn as a function of the amount of introduced steel

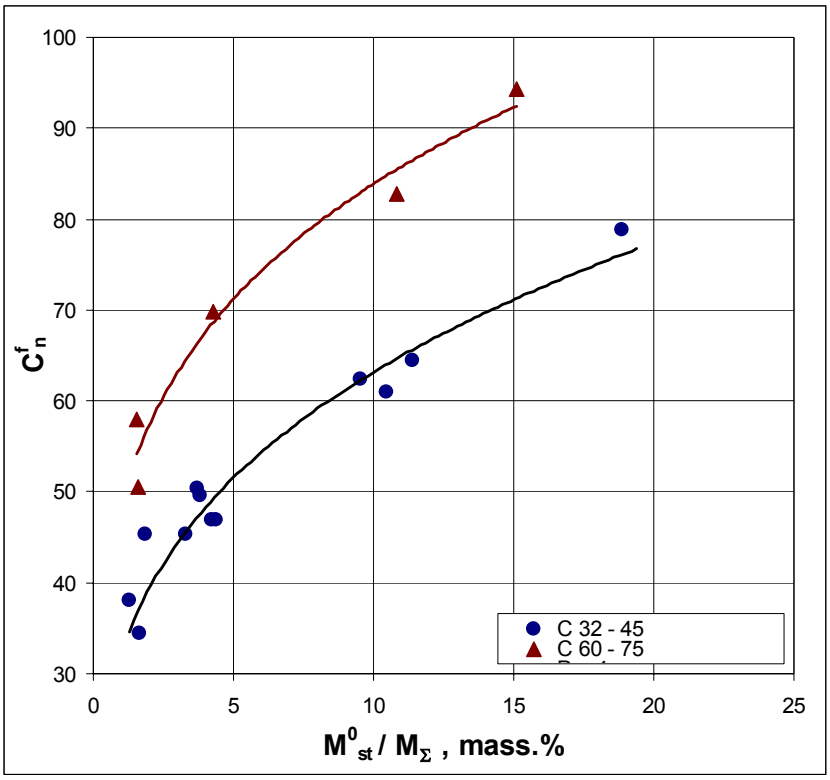

Figure 7. U, Zr and Fe concentrations in the metallic ingot as a function of the amount of introduced steel in the range of C32 -C45

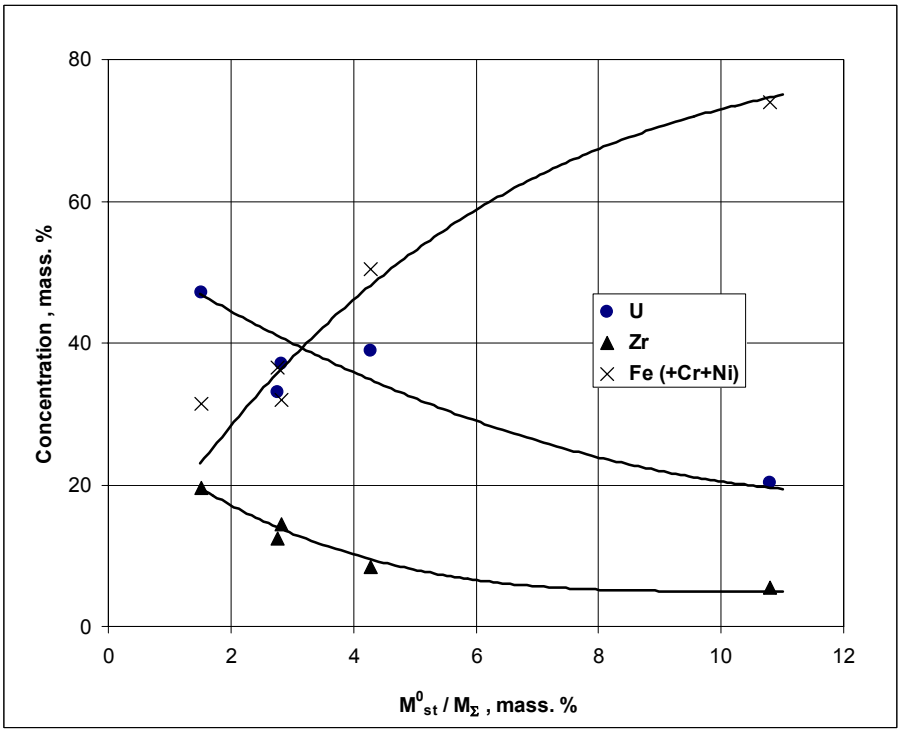

Figure 8. U, Zr and Fe concentrations in the metallic ingot as a function of the amount of introduced steel in the range of C60- C75

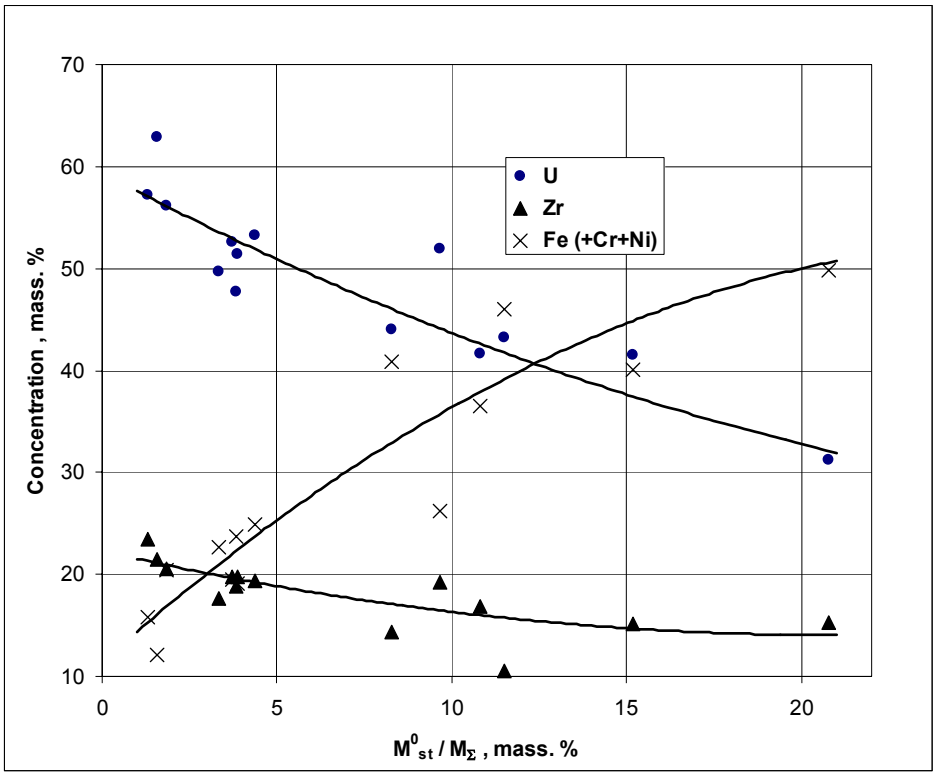

The measured metallic and oxidic part densities are given in Figs. 9, 10. The most relevant factor influencing the metallic phase density increase is the concentration of U transported into it; whereas the oxidic phase density depends on the oxygen concentration. In all conducted tests the density of metallic phase was found to be higher than that of oxidic, and this agrees with the bottom position of the metallic ingot found in all tests. As it has been noted, the only exclusion is MA-2, in which the metallic ingot was extended vertically (Fig. 3). Only in this test the combination of a high initial Zr oxidation degree (~ C75) and a large relative mass of introduced steel (~11 mass.%) caused a comparatively low average concentration of U in the metallic phase of the melt (~20 mass.%) and, correspondingly, comparatively low density of this phase. Measurements have shown (Fig. 9, 10) that the density of ingot top was 7.9 g/cm^3, whereas the average density of the bottom part was 8.66 g/cm^3. These values agree with the metal shape and position found in the ingot. For comparison, in STFM-Fe10 with Cn close to MA-2 (Cn≈70), but the lower $M^0_{st} / M_\Sigma \approx$ 4,5 mass.%, U concentration in the metallic phase was ~ 40 mass.%. In STFM-Fe15 with close to MA-2 $M^0_{st} / M_\Sigma \approx$ 11 mass.%, but lower Cn (Cn≈35), U concentration in the metallic phase was ~ 45 mass.%.

Figure 9. Metal phase density at ambient temperature as a function of U/Steel(Fe) atomic ratio

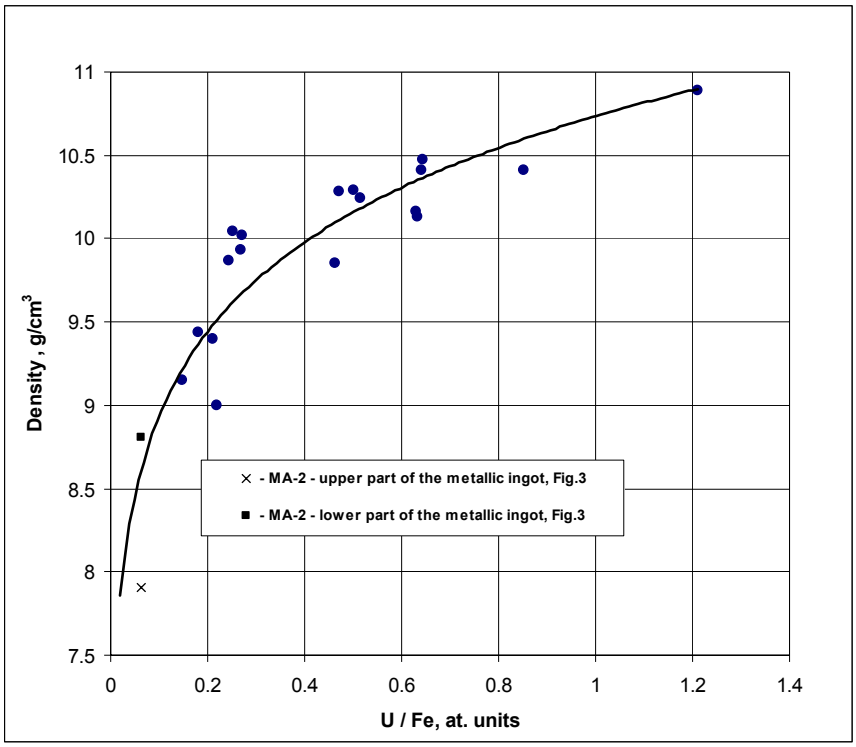

Figure 10. Oxide phase density at ambient temperature as a function of oxygen content

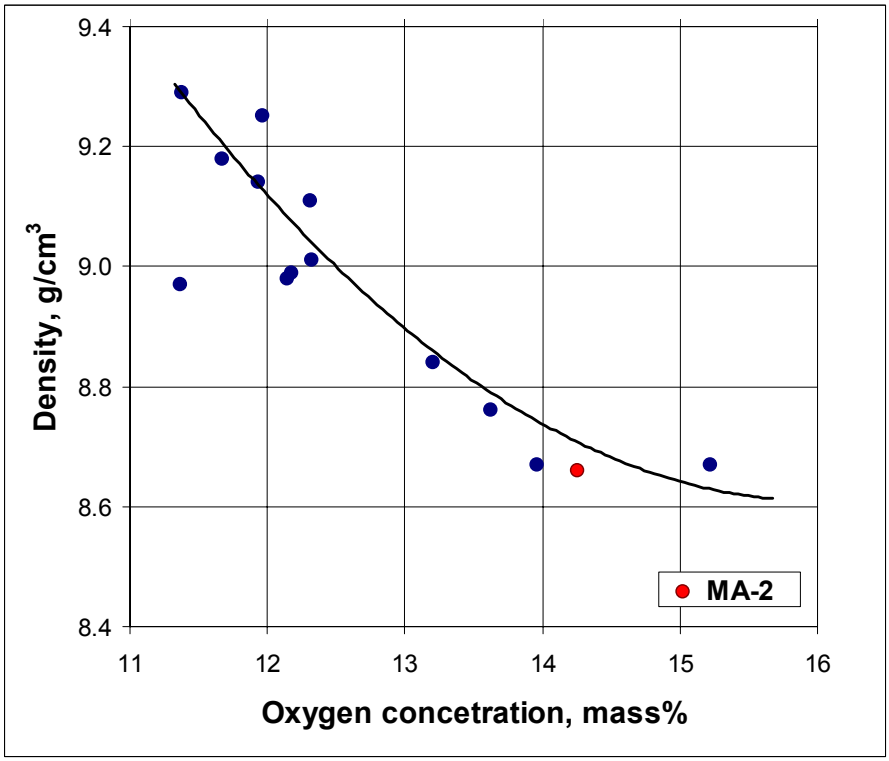

3.2 FP partitioning

The measured concentrations of FP simulants in the oxidic and metallic parts of the STFM-FP and MA-3, 4 ingots demonstrated the qualitative difference in the character of Mo and Ru, and Sr, Ba, Ce, La partitioning. Thus, the Mo and Ru content in the metallic part varies within 1...2 mass.%, and in the oxidic – 0.02...0.1 mass.%. On the opposite, such elements as Sr, Ba, Ce, La are distributed in the following way: in the metallic part of the ingot the content of Sr, Ba, Ce, La is 0.01...0.03 mass.%, and in the oxidic – 0.1...0.7 mass.%.

We can use the partitioning coefficient equal to the ratio of component concentrations in the metallic and oxidic parts of the melt as the parameter characterizing the FP redistribution. Table 3 shows these coefficients for the conducted tests. As the number of independent critical parameters is commensurable with the number of tests, the statistically credible correlations have not been yet established.

Table 3. FP partitioning between the metallic and oxidic phases of the melt

Test	Partitioning coefficients					
	Mo	Ru	Sr	Ba	Ce	La
STMF-FP1	16	16	0.16	0.13	<0.05	0.42
STMF-FP2	34.6	31.6	0.12	0.09	0.1	0.24
STMF-FP3	6.1	11	0.13	0.1	<0.1	0.15
STMF-FP6	14.2	24	0.07	0.025	0.037	0.046
STMF-FP7	61.7	76.2	0.13	0.1	<0.14	0.24
STMF-FP8	50.6	73.3	0.21	0.15	0.3	0.02
MA-3	82	58	0.06	<0.001	0.09	0.09
MA-4	37	56	0.03	0.03	0.03	0.02

The detailed information about the experimental conditions and results of all tests carried out within MASCA-1 is presented in [13].

4. Discussion of Results

The MASCA-1 experimental results have confirmed the existence of a wide miscibility gap region in the corium-steel system. Oxidic and metallic liquids with different densities tend to layer separation. As the concentration of Fe (steel) grows and oxygen potential in the system decreases (Cn decrease), the fraction of U (and Zr) extracted from the oxidic phase into metallic one increases. At the same time, U concentration in the metallic phase, which mostly influences its density, is increased with the decrease of oxygen potential in the system, but it reduces with Fe (steel) concentration growth due to dissolution. It is evident that the independent variation of critical parameters can cause different macrostructures of the molten pool, and at the next phase of the MASCA Project it is planned to conduct tests with increased content of steel. It is also planned to determine the sensitivity of studied phenomena to the U/Zr ratio; it has not been explicitly determined during the 1st phase of MASCA Project.

Although the determined qualitative characteristics seem to be very convincing, the application of quantitative results is possible only after additional discussions. It is very important to estimate to what extent the produced data correspond to the equilibrium conditions. Lack of equilibrium between the liquid and gaseous phases can be neglected, because the typical period of mass exchange between

them is by several orders longer than test duration. On the contrary, the time of establishing thermal stabilization in the melt under the conditions of induction melting in the cold crucible is considerably shorter than test duration. Same applies to the mass exchange processes, which produce crusts on the pool boundaries. The main issue to be dealt with is the establishment of chemical equilibrium between oxidic and metallic liquids, because its time determines the test duration.

In order to check the required test duration the comparison of 3 STFM tests (C32, $M_{st}^{0} / M_{\Sigma} \approx 1.5w\%, U / Zr \approx 1.1, T = 2500°C$) was made – they differed only in duration: 10, 30 and 60 min. Fig. 11 shows their data on U and Zr concentrations in the metallic part of the ingot, they prove that the equilibrium is reached in less than 10 min.

Figure 11. U and Zr content in the metallic ingot after different exposition times in STFM tests

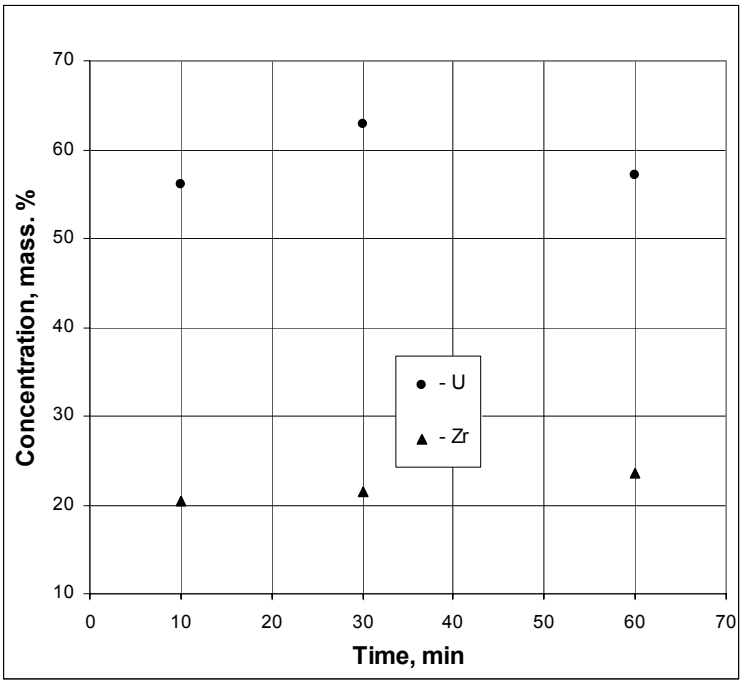

Therefore, the exposition time of ≥ 10 min. in the STFM series and 30 min. in the MA series probably ensures the representative data in terms of establishing equilibrium compositions of metallic and oxidic parts of the melt.

Though the data on the FP simulants partitioning between metallic and oxidic phases are quite scattered, the main conclusion that Ru and Mo concentrate mostly in the metallic part, and Sr, Ba, Ce, La – in the oxidic one enable to considerably improve the forecasts of decay heat distribution in the molten pool in realistic conditions. Along with that, the analysis of FP release (made in the framework of MASCA project) taking into account the presented results enables to more accurately determine their distribution depending on the molten pool structure (relative position of metallic and oxidic phases).

Conclusions

The discovered and quantified phenomena of component partitioning between the oxidic and metallic phases during the interaction of suboxidized corium and steel melts improves the insight into the phenomena taking place at the late stage of a severe accident. Though the obtained experimental data cannot be considered as exhaustive, they can be used in the development and validation of numeric codes modeling physico-chemical processes of the molten pool formation in the reactor vessel. The studies continued in the framework of MASCA-2 project enable to get additional and specify earlier produced experimental data, which eventually contributes to the upgrade of light-water reactors safety level.

REFERENCES

1. O. Kymalainen, H. Tuomisto, T.G. Theofanous «In-Vessel Retention of Corium at the Loviisa Plant», Nuclear Engineering and Design **169** (1997) 109-130.
2. T.G. Theofanous, C. Liu, S. Addition, S. Angelini, O. Kymalainen, T. Salmassi «In-Vessel Coolability and Retention of a Core Melt», Nuclear Engineering and Design. **169** (1997) 1-48.
3. M.F. Rogov et al., «Analyzing the Possibility of Retaining the Corium in the Vessel of a VVER-640 Reactor in a Severe Accident with a Damage Core», Thermal Engineering **44** (1997) 888-892.
4. M. Helle, O. Kymalainen, H. Tuomisto. Experimental Date on Heat Flux Distribution from Volumetrically Heated Pool with Frozen Boundaries. NEA/CSNI/R(98)18. In-Vessel Core Debris Retention and Coolability. Workshop Proceedings, March 3-6 1998, Munich, Germany.
5. L. Bernaz et. al., Thermal hydraulic Phenomena in Corium Pools: Numerical Simulation with TOLBIAC and Experimental Validation with BALI. NEA/CSNI/R(98)18. In-Vessel Core Debris Retention and Coolability. Workshop Proceedings, March 3-6 1998, Munich, Germany.
6. V. Asmolov, Latest Findings from the OECD RASPLAV Project, Proceedings of 24 Water Reactor Safety Meeting, October, 1996, 1, 37-45.
7. T.G. Theofanous, S. Syri. The Coolability Limits of a Reactor Pressure Vessel Lower Head. Proceedings of 7-th International meeting on Nuclear Reactor Thermal-Hydraulics. NURETH-7. New York, September 10-15 1995 (1) 627-647.
8. RASPLAV Final Report. RRC «Kurchatov Institute». July 2000.
9. P. Hofmann, Reaktions-und Schmelzverhalten der LWR-Corekomponenten UO_2, Zircaloy ung Stahe wahrend der Abschmelzperiod, KFK 2220, Juli, 1976.
10. V. Asmolov, Latest Findings of RASPLAV Project NEA/CSNI/R(98). In-Vessel Core Debris Retention and Coolability. Workshop Proceedings, March 3-6 1998, Munich, Germany.
11. B. Eppinger, G. Fieg, S. Schmidt-Stiefel, W. Tromm, Investigations of the metallic and oxidic in-vessel corium densities: GEMINI2 calculations, IKET/FZK Report, September, 2001.
12. N.A. Toropov., V,P. Barzakovsky., I.A. Bondar et al. Phase diagram of silicate systems. Reference book. Second issue. L.: Nauka, 1969. (In Russian)
13. Main Results of the First Phase of MASCA Project. Integrated Report. RRC «Kurchatov Institute». 2004.